



**HAL**  
open science

# Enzyme-Induced Silver Deposition on Gold Nanorods for Naked-Eye and Smartphone Detection of Acrylamide in Food

Hui-Jun Fu, Lin Luo, Yu Wang, Cheng-Long Wang, Hong Wang, Yu-Dong Shen, Hong-Tao Lei, Niko Hildebrandt, Zhen-Lin Xu

► **To cite this version:**

Hui-Jun Fu, Lin Luo, Yu Wang, Cheng-Long Wang, Hong Wang, et al.. Enzyme-Induced Silver Deposition on Gold Nanorods for Naked-Eye and Smartphone Detection of Acrylamide in Food. ACS Applied Nano Materials, 2022, 5 (9), pp.12915-12925. 10.1021/acsanm.2c02763 . hal-03814452

**HAL Id: hal-03814452**

**<https://normandie-univ.hal.science/hal-03814452v1>**

Submitted on 26 Jan 2023

**HAL** is a multi-disciplinary open access archive for the deposit and dissemination of scientific research documents, whether they are published or not. The documents may come from teaching and research institutions in France or abroad, or from public or private research centers.

L'archive ouverte pluridisciplinaire **HAL**, est destinée au dépôt et à la diffusion de documents scientifiques de niveau recherche, publiés ou non, émanant des établissements d'enseignement et de recherche français ou étrangers, des laboratoires publics ou privés.

# **Enzyme-Induced Silver Deposition on Gold Nanorods for Naked-Eye and Smartphone Detection of Acrylamide in Food**

Hui-Jun Fu<sup>a,b</sup>, Lin Luo<sup>a</sup>, Yu Wang<sup>c</sup>, Cheng-Long Wang<sup>c</sup>, Hong Wang<sup>a</sup>, Yu-Dong Shen<sup>a</sup>,  
Hong-Tao Lei<sup>a</sup>, Niko Hildebrandt<sup>b,d,e\*</sup>, Zhen-Lin Xu<sup>a,\*</sup>

<sup>a</sup> Guangdong Provincial Key Laboratory of Food Quality and Safety/ Guangdong Laboratory of Lingnan Modern Agriculture, South China Agricultural University, Guangzhou 510642, China.

<sup>b</sup> nanofret.com, Laboratoire COBRA, UMR6014 & FR3038, Université de Rouen Normandie, CNRS, INSA, Normandie Université, 76000 Rouen, France.

<sup>c</sup> Guangzhou Institute of Food Inspection, Guangzhou 510410, China.

<sup>d</sup> Department of Chemistry, Seoul National University, Seoul 08826, South Korea.

<sup>e</sup> Université Paris-Saclay, 91405 Orsay Cedex, France.

\*Corresponding authors: Niko Hildebrandt ([niko.hildebrandt@univ-rouen.fr](mailto:niko.hildebrandt@univ-rouen.fr)) and Zhen-

Lin Xu ([jallent@163.com](mailto:jallent@163.com))

## **ABSTRACT**

Acrylamide is a probable human carcinogen with wide occurrence in commonly consumed food. Owing to the lack of specific antibodies against acrylamide, immunoassays usually measure acrylamide derivatives, which require long derivatization times at elevated temperatures. One exception is xanthyl acrylamide (XAA), which can be derived from acrylamide at room temperature within 30 min. Here, we present the development of a monoclonal antibody against XAA and a competitive enzyme-linked immunosorbent assay (ELISA) based on multicolor detection of gold nanorods (AuNRs). The biotinylated monoclonal antibodies bound streptavidin alkaline phosphatase, which induced XAA concentration-dependent silver deposition on the AuNRs. The resulting blue-shift of the AuNR surface plasmon resonance peak translated into a strong gray-to-orange color change that could be conveniently distinguished by the naked eye or smartphone color detection. The assay showed a broad linear range (0.3 to 17.2 ng/mL), a low limit of detection (0.06 ng/mL), and a 3.6-fold sensitivity improvement compared to conventional tetramethylbenzidine-based ELISA. The analysis of several different food products showed excellent acrylamide concentration recoveries (84% to 102%) and confirmed the applicability as an effective tool for routine monitoring of acrylamide in food. Rapid and simple color analysis demonstrated the strong potential for implementation into direct consumer product testing.

**Keywords:** acrylamide, multicolor immunoassay, nanoparticles, semi-quantitative

## INTRODUCTION

Acrylamide is a chemical compound with 71Da molecular weight and easily generated from baked and fried food during high-temperature treatment (above  $\sim 120^{\circ}\text{C}$ ) due to the Maillard reaction.<sup>1</sup> Many studies have shown that acrylamide has genotoxicity,<sup>2,3</sup> carcinogenicity,<sup>4,5</sup> and neurotoxicity.<sup>6,7</sup> In 1994, acrylamide was classified as probable human carcinogen in group 2A by the International Agency for Research on Cancer (IARC).<sup>8</sup> In 2002, the Swedish national food administration and the University of Stockholm announced the wide presence of acrylamide in foods under high-temperature preparation.<sup>9</sup> In 2016, the U.S. Food and Drug Administration (FDA) issued guidelines for acrylamide mitigation,<sup>10</sup> followed by the European Regulation (EU) 2017/2158 to establish both mitigation measures and benchmark levels in food products,<sup>11</sup> such as baby food ( $< 150$  ng/g), coffee (400-800 ng/g), biscuits (300-800 ng/g), and French fries/slices (500-750 ng/g). Although currently no maximum residue level (MRL) for acrylamide in food products has been set, the knowledge of acrylamide levels is essential for determining the effectiveness of acrylamide reduction techniques in order to mitigate the daily exposure. Therefore, economic, rapid, and portable methods for determining acrylamide contents in foods are highly desirable.

To date, analytical techniques for the quantification of acrylamide in foods are mainly based on chromatography, e.g., high-performance liquid chromatography (HPLC), gas chromatography (GC), or GC/LC coupled with mass spectrometry (GC-MS, LC-MS).<sup>12,13</sup>

Such methods, are sensitive and selective but also time-consuming, expensive, and require highly trained personnel. Thus, it is difficult to accomplish frequent monitoring of a large number of samples. In contrast, immunoassays are simple, rapid, sensitive, and cost-effective techniques, which were also proposed by the FDA to monitor acrylamide in food samples.<sup>10</sup>

Studies based on specific antibodies for detecting acrylamide have been reported.<sup>14,15</sup> However, only few antibodies can directly recognize acrylamide and the insufficient epitope of the low molecular weight acrylamide strongly limits a reproducible production of specific antibodies and their application for reproducible immunoassays.<sup>16-18</sup> As a consequence, acrylamide immunoassays are mainly based on antibodies against acrylamide derivatives. However, common derivatization reactions, which use 3-mercaptopbenzoic acid<sup>19</sup> or 4-mercaptopbenzoic acid<sup>15</sup> result in low efficiency and relatively long reaction times (over 1h) with the necessity of heating (over ~50°C). One exception is xanthyl acrylamide (XAA), which can be derived from acrylamide within only 30 min at room temperature, using xanthidrol as derivatization reagent. Recently, our group obtained a specific polyclonal rabbit antibody against XAA to develop more rapid and simple immunoassays for acrylamide.<sup>20</sup> Unfortunately, polyclonal antibodies suffer from strong batch-to-batch differences, which limit their application in reproducible immunoassays, and the development of monoclonal antibodies is highly desirable.

Conventional immunoassays based on colorimetric or luminescence readout are most

often based on laboratory operations as well as professional instruments,<sup>21,22</sup> which usually provide them with high diagnostic performance but also with shortcomings concerning on-site sample analysis. Naked-eye or smartphone-based analyses are usually less precise but may be sufficient for certain applications and come with the great advantage of simplicity, low cost, and rapidity for on-site monitoring. Gold nanomaterials play an important role in naked-eye detection platforms,<sup>23-26</sup> owing to their unique properties, such as facile synthesis, shape- and size-dependent optical absorption, and high absorption cross sections. It was shown that the localized surface plasmon resonance (LSPR) absorption of gold nanorods (AuNRs) is extremely sensitive to shape, size and shell composition (such as silver coating). Multicolor immunoassays were developed for the visual analysis of carcinoembryonic antigen, prostate-specific antigen (PSA),<sup>27</sup> and HIV-1 p24 antigen.<sup>28</sup> These assays were based on horseradish peroxidase (HRP)-labeled antibodies to quantitatively etch AuNRs via the generated 3,3',5,5'-tetramethylbenzidine<sup>2+</sup> (TMB<sup>2+</sup>). Etching AuNRs via H<sub>2</sub>O<sub>2</sub> combined with Fe<sup>2+</sup> for decomposing H<sub>2</sub>O<sub>2</sub> to generate strong oxidative hydroxyl radicals ( $\cdot$ OH) was applied for constructing multicolor assays for aflatoxin B<sub>1</sub>, alpha-fetoprotein, and microRNA.<sup>29</sup> Enzyme-mediated Ag deposition on AuNRs is another approach for the design of multicolor immunoassays. This method was applied for visual detection of the H<sub>5</sub>N<sub>1</sub> virus and PSA.<sup>30,31</sup> Overall, AuNRs modification by etching or deposition could result in significant color variations for eliminating background interference and improving the sensitivity of immunoassay.<sup>32-34</sup>

Herein, with the aim to accomplish a more convenient and sensitive assay for acrylamide, we developed a monoclonal antibody (mAb) against XAA. The mAb was biotinylated (biot-mAb) and applied in a simple naked-eye or smartphone-based immunoassay. The combination of biot-mAb and the quantification via Ag deposition on AuNRs resulted in significant improvements concerning simplicity and sensitivity of acrylamide analysis. The analytical performance was evaluated and the applicability to real-life acrylamide screening was demonstrated by quantification in food samples.

## **MATERIALS AND METHODS**

**Materials and reagents.** Acrylamide, ethyl carbamate, methyl carbamate, acrylic acid, methyl acrylate, methacrylamide, and L<sup>(+)</sup> ascorbic acid (AsAc) were purchased from Aladdin Chemical Technology Co., Ltd. (Shanghai, China). Hexadecyl trimethyl ammonium bromide (CTAB), sulfo-NHS-biotin, and sodium borohydride (NaBH<sub>4</sub>) were provided by Shanghai Macklin Biochemical Co., Ltd. (Shanghai, China). 2-phospho-L-ascorbic acid trisodium salt (AsAcP), streptavidin-alkaline phosphatase (SA-ALP), bovine serum albumin (BSA), and ovalbumin (OVA) were purchased from Sigma-Aldrich (China). Silver nitrate (AgNO<sub>3</sub>) and gold (III) chloride trihydrate (99.9%, H<sub>2</sub>AuCl<sub>4</sub>·4H<sub>2</sub>O) were provided by Sinopharm Chemical Reagent Co., Ltd. (China). All chemicals and reagents were used in analytical grade. Antibody and antigen were prepared in our lab. The dialysis membrane was provided by Yuanye Bio-Technology Co., Ltd (Shanghai, China). PES

filters (0.22  $\mu\text{m}$ ) were purchased from Jinteng experimental equipment Co., Ltd (Tianjin, China).

**Instruments.** SpectraMax i3x multi-function detection platform (Molecular Devices, USA) was used for absorption spectra measurements. The sizes and morphologies of AuNRs were characterized by transmission electron microscopy (TEM, Tecnai G2 F30 S-TWIN, and FEI, USA). The concentration of proteins were quantified by NanoDrop 2000C system (thermo scientific, USA). Ultra-performance liquid chromatography-quadrupole/orbitrap high-resolution mass spectrometry (UPLC-Q-Orbitrap HRMS, Thermo Fisher, USA) was used for analytical comparison.

**Preparation of AuNRs.** AuNRs were synthesized using the seed-mediated growth method as reported previously.<sup>27</sup> Briefly, freshly prepared cold  $\text{NaBH}_4$  (600  $\mu\text{L}$ , 0.01 mol/L, 4°C) was rapidly added into a solution composed of 0.2 mol/L CTAB (5 mL) and 10 mmol/L  $\text{HAuCl}_4$  (250  $\mu\text{L}$ ). After vigorous stirring for 2 min, the color of the seed solution changed from yellow to brown. Then the mixture was finally stirred gently for 1h at room temperature. For the growth solution preparation,  $\text{HAuCl}_4$  (2.5 mL, 0.01 mol/L) and  $\text{AgNO}_3$  (400  $\mu\text{L}$ , 0.01 mol/L) were mixed with the CTAB (50 mL, 0.1 mol/L). The AsAc (325  $\mu\text{L}$ , 0.1 mol/L) was slowly dropped into the mixture resulting in the color of solution changing from yellow to colorless. Subsequently, the seed solution (50  $\mu\text{L}$ ) was injected into the above growth solution. After vigorously stirring for 30 s, the preparation was incubated at 30°C for 12 h. The obtained AuNRs were centrifuged for 15 min at 5342 g

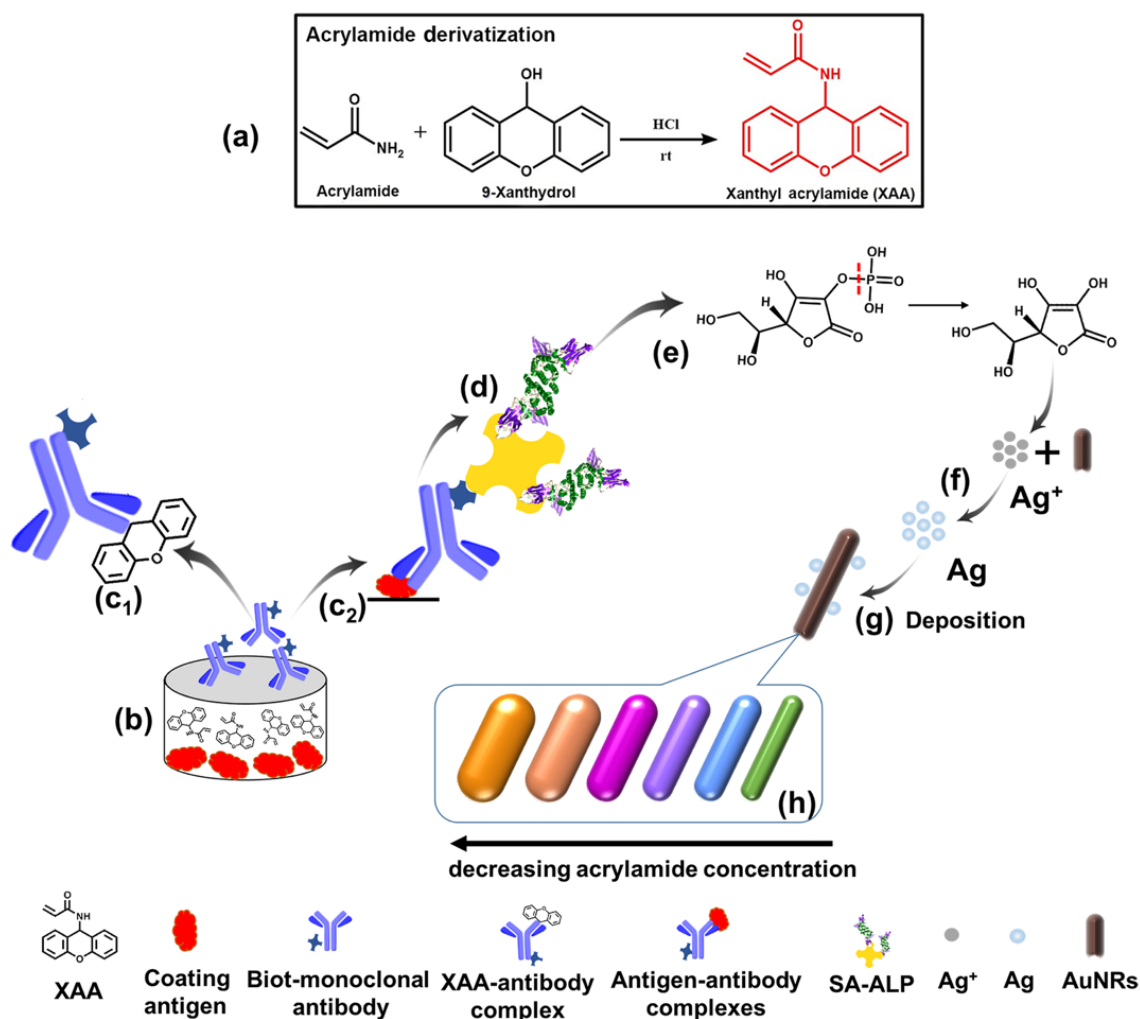


followed by removal of the supernatant. The obtained AuNRs were washed twice using the 50 mL of 0.06 mol/L CTAB solution under the same centrifuge condition. Finally, precipitation was suspended into 10 mL of ultra-pure water and kept at room temperature.

**Production and biotinylation of anti-XAA-mAb.** Details of production and purification of antigen and anti-XAA-mAb are shown in the Supporting Information. 200  $\mu$ L of purified anti-XAA-mAb (200  $\mu$ L, 5 mg/mL) was reacted with sulfo-NHS-biotin (1mg/mL, dissolved in 0.01mol/L PBS), stirring at 4°C for 12 h. Then the mixture was dialyzed in PBS (0.01 mol/L, pH 7.4) for 12 h. Dialysis was performed using a 8 kDa -12 kDa cutoff membrane. Finally, the prepared biot-mAb was kept at 4 °C until use.

**Procedure of derivatization and multicolor immunoassay.** As illustrated in **Scheme 1**, competitive binding of XAA and coating antigen to biot-mAb specific for XAA can result in concentration-dependent streptavidin-alkaline phosphatase binding. AsAcP as the substrate can be hydrolyzed into AsAc, leading to the reduction and then deposition of silver (Ag) on the AuNRs. Modification with Ag on the AuNRs can result in a strong blue shift of the longitudinal LSPR peak and a concomitant color change that strongly depends on the acrylamide concentration. First, coating antigen (100  $\mu$ L, 1  $\mu$ g/mL) was incubated into the 96-microwell plate overnight at 37°C. The nonspecific sites were blocked by using 0.01 mol/L PBS containing 3% skimmed milk for 3 h after 2 times washing with PBST. Derivatizing agent 9-xanthidrol (400  $\mu$ L, 4 mg/mL) prepared in acetonitrile was mixed with 600  $\mu$ L of a serial concentration of acrylamide standards. Then HCl (100  $\mu$ L, 1.5

mol/L) was added to trigger the derivatization. After a 30-min reaction, derivatization was terminated by adding 0.1 mL of NaOH (1.5 mol/L). The mixture was subsequently diluted 5-fold with PBS, which was used as competitor for the following multicolor immunoassay analysis. The biot-mAb (1  $\mu\text{g/mL}$ , 50  $\mu\text{L/well}$ ) and an equal volume of analyte in PBS or PBS alone were added into coated wells with 30 min incubation at 37  $^{\circ}\text{C}$ . Afterwards, the wells were washed five times with 0.05% PBST. SA-ALP (100  $\mu\text{L/well}$ ) was added to each well for 30 min incubation at 37  $^{\circ}\text{C}$ , followed by five times washing. TBST-containing AsAcP was added (100  $\mu\text{L}$  per well) and incubated for 40-min at 37  $^{\circ}\text{C}$  for forming AsAc. The mixture (18  $\mu\text{L}$  per well) composed of as-prepared AuNRs (15  $\mu\text{L}$ ) and  $\text{AgNO}_3$  (3  $\mu\text{L}$ ) were added into the covered wells and incubated for 10 min at room temperature. The UV-vis absorption spectra within the range of 300 nm to 800 nm of the solution were measured.



**Scheme 1.** Schematic principle of the multicolor immunoassay for acrylamide analysis. After acrylamide derivatization for 30 min (a), XAA and biot-mAb were incubated for 30 min in antigen-coated microwell plates (b). XAA-antibody complexes were washed out (c<sub>1</sub>) and the remaining biot-mAb was bound to antigen on the plate (c<sub>2</sub>). After washing, the antigen-antibody complexes could bind with SA-ALP after 30 min of incubation (d). After washing, the wells were incubated with 2-phospho-L-ascorbic acid trisodium salt for 40 min, which resulted in the formation of AsAc (e). AuNRs and AgNO<sub>3</sub> were added and Ag<sup>+</sup> was reduced to Ag by AsAc (f), which resulted in the formation of an Ag shell on the AuNRs (g) and an acrylamide concentration-dependent color change (h) caused by the different Ag shell thicknesses.

**Sample analysis.** For sample analysis, normal food samples were obtained from a local shop in Guangzhou, China. The samples were analyzed by UPLC-Q-Orbitrap HRMS and

the one with the lowest background level of acrylamide was applied for performing spiked sample experiments. For sample preparation for UPLC-Q-Orbitrap HRMS and immunoassay, briefly, crushed fully sample (10 g) was dissolved in 40 mL methanol. After thorough mixing and centrifugation at 2100 g for 5 min, filtered (by 0.22  $\mu\text{m}$  PES filter) supernatant (20 mL) was dried with nitrogen at 25°C. The product was resolved in 5 mL distilled water. In order to remove influence of grease, *N*-hexane (5 mL) was added subsequently. Finally, take the 0.6 mL of water layer and submit to UPLC-Q-Orbitrap HRMS analysis or derivatization for further immunoassay analysis. The details of UPLC-Q-Orbitrap HRMS analysis are shown in the Supporting Information.

## RESULTS AND DISCUSSION

**Production and characterization of monoclonal antibodies.** To reduce the derivatization time for acrylamide detection, we used xanthidrol as derivatizing agent. The antiserum of mice immunized was collected and characterized by indirect competitive ELISA (ic-ELISA) with two coating antigens using XAA (**Supporting Figure S1**) after the 4th immunization. While all three antisera displayed a certain affinity for XAA, #3 showed the highest affinity and the inhibition reached 69% in the presence of 100 ng/mL XAA with 295-OVA as coating antigen (**Table 1**). Thus, the spleen cells of #3 mice and 295-OVA were selected for hybridoma preparation and as coating antigen, respectively. To obtain a mAb with the highest sensitivity, XAA was used as a competitor and the concentration of

XAA decreased for each round of subclonal screening. Ultimately, the obtained mAb was purified and identified by 12% SDS-PAGE (**Supporting Figure S2**).

**Table 1.** Characterization of antiserum against XAA using homologous and heterologous coating antigens.

Coating antigen (1000 ng/mL)	#1 <sup>a</sup>		#2		#3	
	Titer <sup>b</sup>	Inhibition <sup>c</sup>	Titer	Inhibition	Titer	Inhibition
	( $\times 10^3$ )	(%)	( $\times 10^3$ )	(%)	( $\times 10^3$ )	(%)
295-OVA	16	43	32	60	64	69
309-OVA	64	22	128	20	128	34

<sup>a</sup>#1, the antiserum is from NO.1 mice immunized. <sup>b</sup>Titer is defined as dilution factor of antiserum with absorbance at 450 nm being from 1.0 to 1.5. <sup>c</sup>Percentage inhibition was calculated as follow: Inhibition (%) =  $[1-(B/B_0)] \times 100$ . B<sub>0</sub> was mean absorbance of the wells with no XAA; B was mean absorbance of the wells with 100 ng/mL XAA as competitor.

Previous studies have shown that using polyHRP to label streptavidin (SA) for reacting with biotinylated antibodies can effectively amplify the signal and improve the sensitivity of the immunoassay.<sup>35</sup> Inspired by this approach, the SA-ALP was applied for improving the sensitivity instead of using traditional goat anti-mouse IgG labeled ALP as secondary antibody. Moreover, the small size (244 Da) and high affinity of biotin for SA can result in efficient SA binding without influencing the biological activity of the assay. Biotinylated mAbs were prepared as described in the Materials and Methods section. Results of ciELISA using SA-HRP as tracer indicated that the biotinylation was successful.

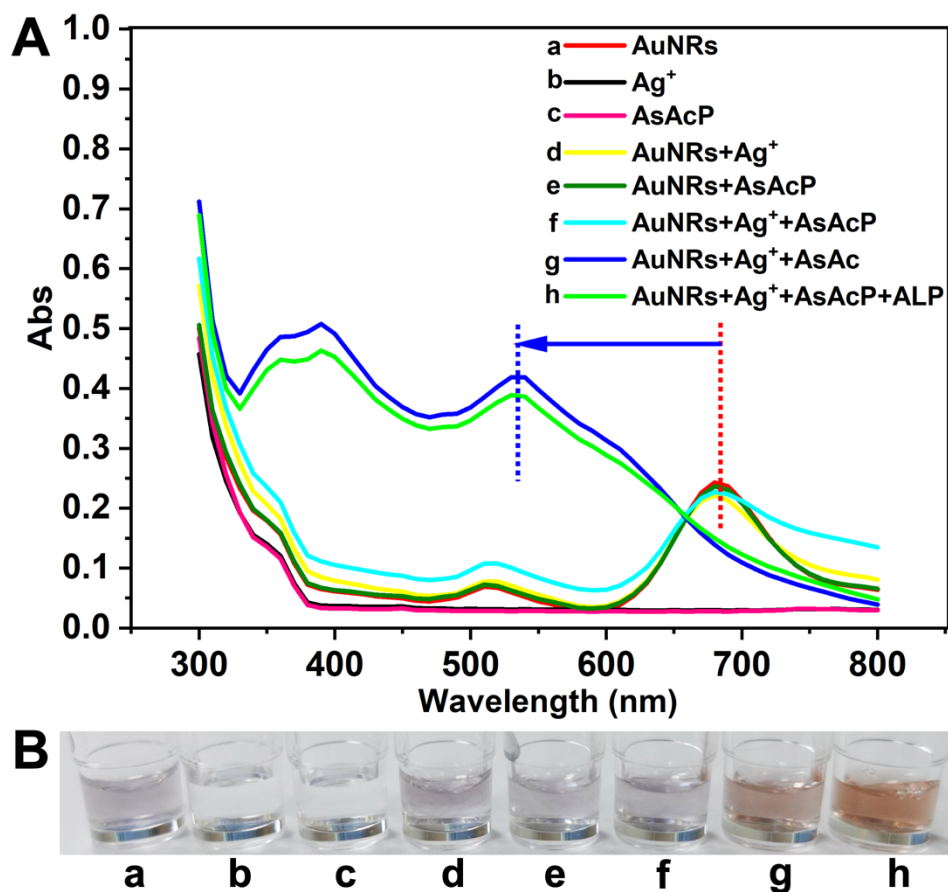


**Figure 1.** UV-vis spectra (A) and images (B) of solutions containing AuNRs, Ag<sup>+</sup>, AsAcP, or mixtures thereof. Curves a, d, and e and curves b and c largely overlap and are therefore not very well distinguishable. The shift of the longitudinal peak is indicated by the blue arrow. AsAcP: 1mmol/L; Ag<sup>+</sup>: 50 mmol/L; SA-ALP: 3 μg/mL; TBST buffer: 5 mmol/L Tris containing 20 mmol/L Mg<sup>2+</sup>, and 0.05% Tween 20, pH 8.0; reaction time: 10 min.

**Feasibility of multicolor immunoassay using ALP.** To verify silver deposition on AuNRs and the concomitant color change, we characterized as-prepared AuNRs under different conditions by UV-vis absorption spectroscopy (**Figure 1**) and TEM (**Figure 2**). The AuNRs UV-vis spectrum (red curve in **Figure 1A**) presented two characteristic absorption peaks at ~510 nm (transverse LSPR peak) and ~690 nm (longitudinal LSPR peak). Negligible absorption in the 400 nm to 800 nm range was observed for Ag<sup>+</sup> (black curve

in **Figure 1A**) and AsAcP (magenta curve in **Figure 1A**). Two characteristic absorption peaks of AuNRs did not significantly change when AsAcP and  $\text{Ag}^+$  were introduced separately (yellow and dark green curves in **Figure 1A**) or simultaneously (cyan curve in **Figure 1A**) to the AuNRs solution. The color of all AuNRs containing solutions was pink (a, d, e, and f in **Figure 1B**), which demonstrated that the reagents showed no color interference with the characteristic peaks of AuNRs. In contrast, the addition of both SA-ALP and AsAcP (green curve in **Figure 1A**) resulted in a strong blue shift and intensity increase of the longitudinal LSPR band from  $\sim 690$  nm to  $\sim 520$  nm accompanied by a strong color change from pink to orange (h in **Figure 1B**). The absorption spectrum and color of a mixture composed of AuNRs,  $\text{Ag}^+$ , and AsAc (blue curve in **Figure 1A** and g in **Figure 1B**) confirmed that ALP could hydrolyze AsAcP into AsAc. TEM and EDX images revealed the morphological change of AuNRs upon Ag deposition via the deposition of a thick Ag shell around the AuNRs (**Figure 2**). Our measurements showed that mainly the diameter of the AuNRs increased, whereas the length was less affected. This effect may be related to less efficient growth on areas with high curvature (at the tip of the AuNRs), which was previously found to reshape the morphology of Au nanostructures.<sup>36</sup> Overall, the obtained results suggested that ALP could hydrolyze AsAcP into AsAc, which resulted in the reduction of  $\text{Ag}^+$  and the formation of an Ag shell on the AuNRs surface. Therefore, SA-ALP should be suitable for XAA target analysis in combination with biot-mAb.

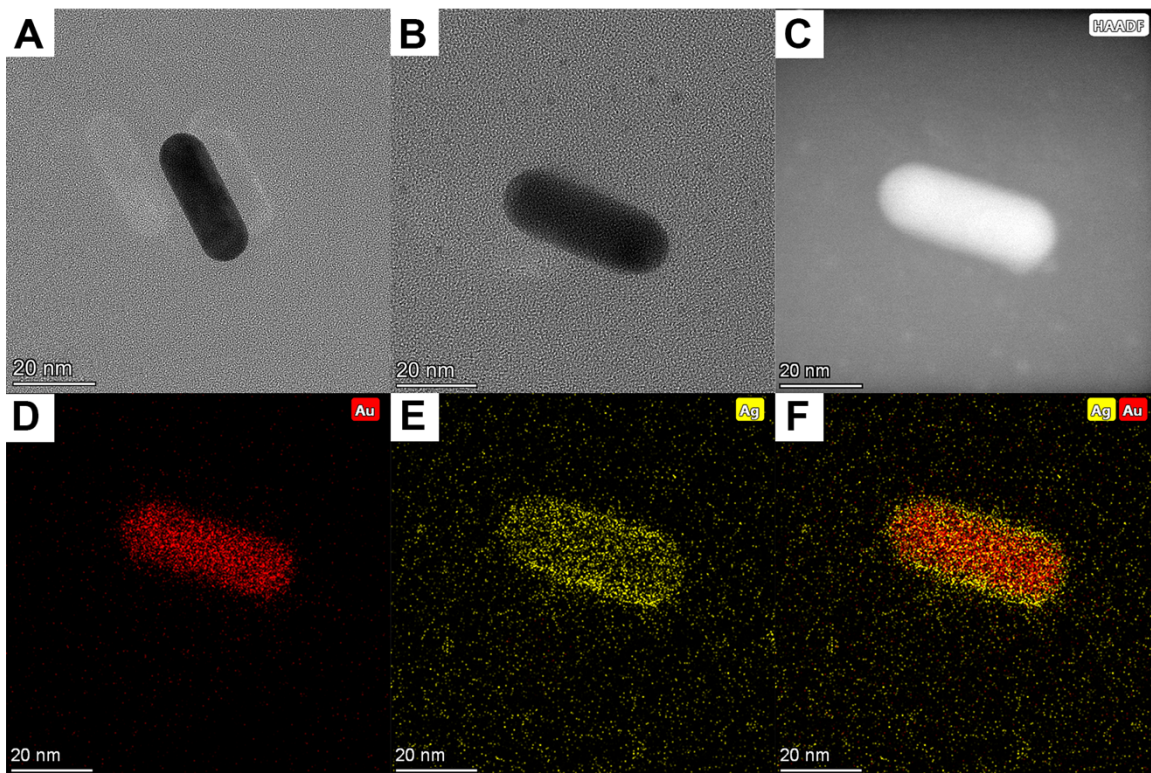


**Figure 2.** TEM images of AuNRs (A) and AuNRs after Ag deposition (B), HAADF-STEM image (C) and corresponding EDX element mapping images of Au (D), Ag (E), and their overlay (F).

**Optimization of multicolor immunoassay conditions.** The proposed multicolor immunoassay depends on the Ag deposition on AuNRs via SA-ALP enzyme-based hydrolyzation of AsAcP to AsAc, which, in turn, depends on the amount of biot-mAbs bound to the coating antigen (in competition with XAA) in the microwells (**Scheme 1**). We therefore optimized several influence factors, including the concentration of AsAcP (5, 2, 1, 0.5, 0.25 mmol/L) and  $\text{Ag}^+$  (40, 20, 10, 5, 2.5 mmol/L), the pH (7.6, 8.3, 9, 9.7 and 10.4) in the AsAcP dilution buffer, and the concentration of SA-ALP (dilution of the 1 mg/mL stock solution in multiples of 300, 600, 1200, 2400, and 4800). The performance of the deposition reaction was evaluated by measuring the blue-shifts of the longitudinal LSPR



peak  $\Delta\lambda$  ( $\Delta\lambda = \lambda_0 - \lambda$ ), where  $\lambda_0$  and  $\lambda$  are the wavelengths of the longitudinal LSPR peaks of AuNRs and AuNRs@Ag, respectively.  $\Delta\lambda$  exhibited a maximum value when the AsAcP concentration reached 1 mmol/L and excessive AsAcP concentrations (2 and 5 mmol/L) inhibited the formation of the LSPR peak (**Figure 3A**). Therefore, an AsAcP concentration of 1 mmol/L was used for the immunoassays. The pH value of AsAcP buffer for deposition reaction also significantly impacted ALP activity.  $\Delta\lambda$  gradually increased with the pH increasing from 7.6 to 9.7 and successively decreased for a pH of 10.4 (**Figure 3B**). The assay performed best at pH 9.7, as expected from the effective pH value for SA-ALP of 9.7 according to the manufacturer. Higher pH (10.4) most probably resulted in the formation of AgOH, which inhibited the deposition process. Thus, we selected pH 9.7 for the immunoassays. As shown in **Figures 3C/D**, the optimal  $\text{Ag}^+$  concentration for maximizing  $\Delta\lambda$  was found to be 20 mmol/L, whereas the optimal SA-ALP dilution was 300-fold in TBST (5 mmol/L Tris containing 20 mmol/L  $\text{Mg}^{2+}$ , and 0.05% Tween 20, pH 8.0). In summary, 1 mmol/L of AsAcP, pH 9.7, 20 mmol/L of  $\text{Ag}^+$ , and 3.3  $\mu\text{g/mL}$  SA-ALP were determined as optimal conditions for the immunoassays.

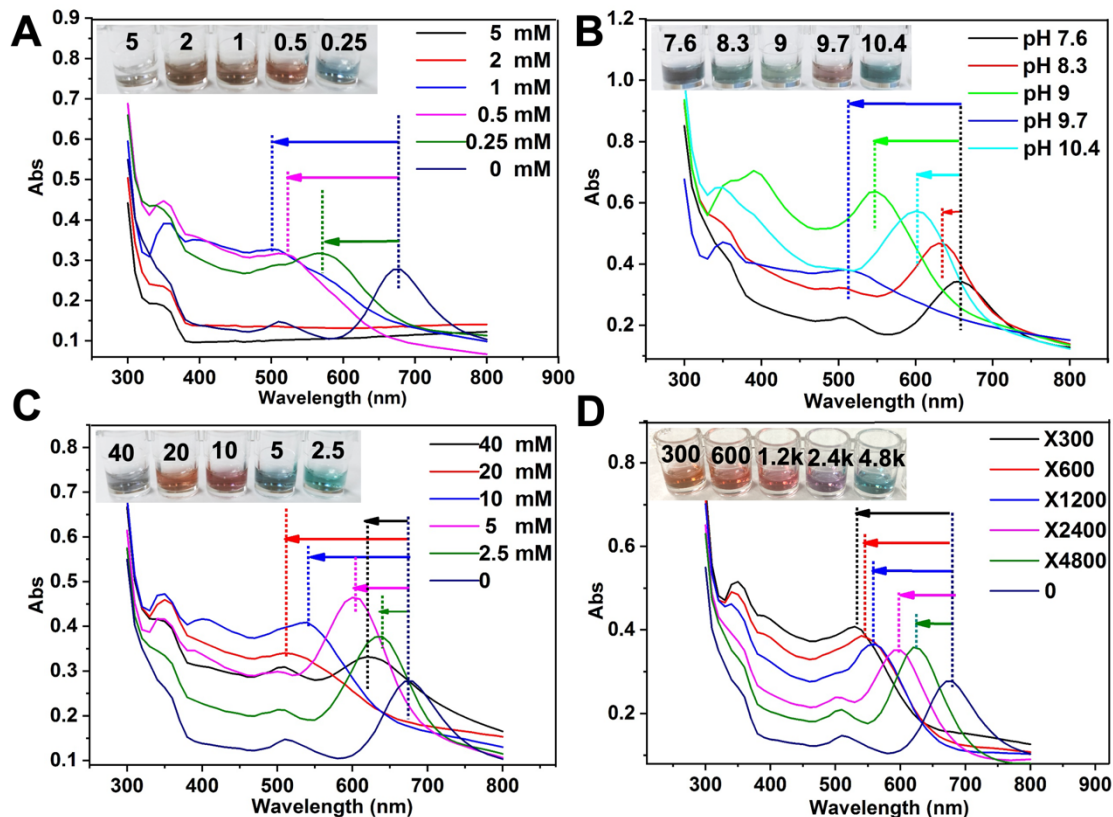


**Figure 3.** UV-vis spectra and images (insets) of assay solutions for different optimization conditions. Effect of AsAcP concentration (A), pH of the detection solution (B), concentration of  $\text{Ag}^+$  (C), and dilution factor of SA-ALP (D). The blue shift of the longitudinal LSPR peaks ( $\Delta\lambda$ ) is indicated by the arrows between the dotted lines.

**Sensitivity and specificity of multicolor immunoassay for acrylamide analysis.** The analytical performance of the multicolor immunoassay was evaluated in a 0 to 20 ng/mL acrylamide concentration range (using acrylamide standards in PBS). The calibration curve was obtained by measuring the blue-shift of the longitudinal LSPR peak ( $\Delta\lambda$ ) against acrylamide concentration. Owing to competition with the coating antigen, increasing acrylamide concentrations resulted in decreasing numbers of biot-mAb in the wells. Thus, less SA-ALP could bind to biot-mAb, which led to decreasing SA-ALP-mediated

hydrolyzation of AsAcP to AsAc. Consequently, AsAc could reduce less  $Ag^+$  to Ag, which resulted in thinner Ag nanoshells on the AuNRs and a concomitant decrease of  $\Delta\lambda$  with increasing acrylamide concentration.

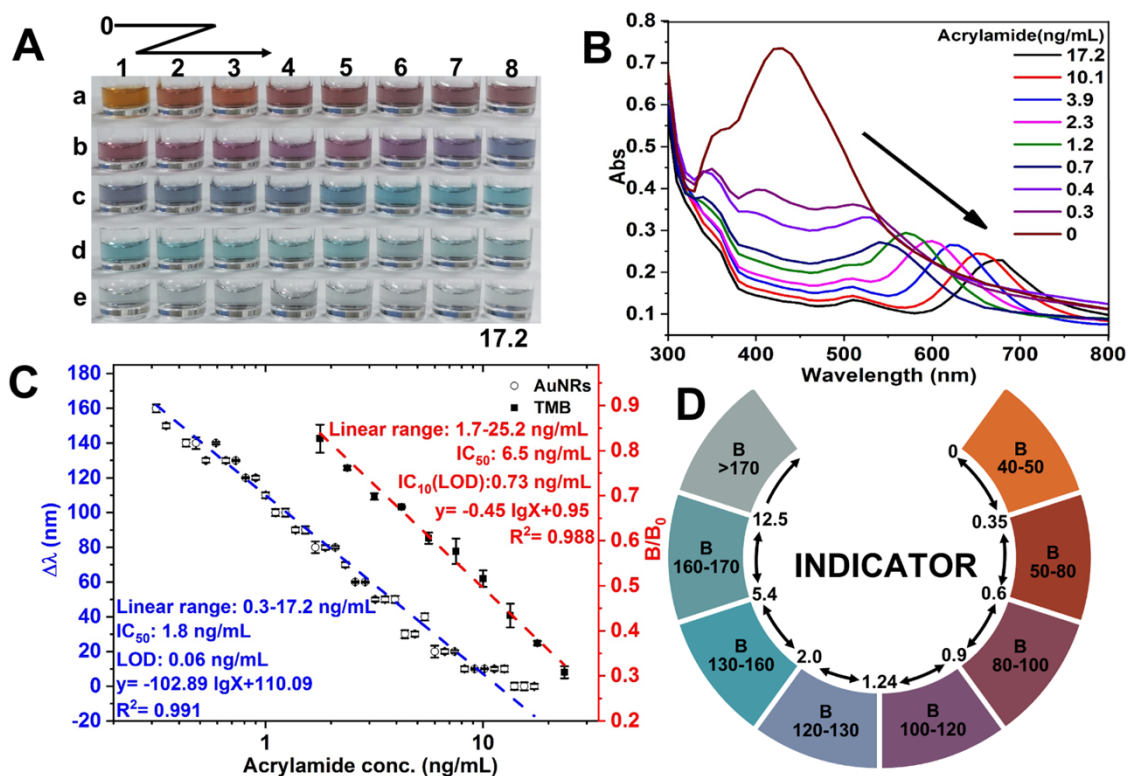


**Figure 4.** Calibration of multicolor immunoassay. A: Images of solutions (with acrylamide concentrations ranging from 0 to 17 ng/mL to be within the linear concentration range of the commercial ELISA) used for calibration (corresponding concentrations are shown in **Supporting Table S1**). B: UV-vis spectra of selected solutions from A (selected such that their absorption spectra were well distinguishable). C: Assay calibration curves of multicolor (blue) and conventional TMB (red) immunoassay. Error bars show standard deviation ( $n=3$ ). D: Color indicator card including the blue value range of the RGB image and concentration ranges in ng/mL for naked-eye or smartphone semiquantitative analysis.

The acrylamide concentration-dependent color changes of the solutions ranged from orange to gray (**Figure 4A**), which was spectroscopically translated into an acrylamide

concentration-dependent significant red-shift and intensity decrease of the longitudinal LSPR peak ( $\Delta\lambda$ ) in the UV-vis absorption spectrum (**Figure 4B**), as expected from decreasing Ag deposition on the AuNRs. In contrast to AuNR size control via etching (e.g., by the commercial TMB-H<sub>2</sub>O<sub>2</sub> system),<sup>27,32</sup> which would lead to increasing intensities with increasing acrylamide concentrations, the high absorption intensities at low concentrations for our deposition approach can significantly increase the signal-to-background ratio and thereby detect lower acrylamide concentrations.<sup>37-39</sup> For evaluating the sensitivity of the assay, the IC<sub>50</sub> (value of acrylamide concentration leading to a 50% decrease in  $\Delta\lambda$ ) of the standard curve was determined. The limit of detection (LOD) was calculated as three standard deviations of the blank control sample (no acrylamide) divided by the slope of the calibration curve. As shown in **Figure 4C**, the multicolor immunoassay exhibited an IC<sub>50</sub> of 1.8 ng/mL, an LOD of 0.06 ng/mL, and a “linear” (with logarithmic concentration) signal decrease range from 0.3 to 17.2 ng/mL ( $y = -102.9 \lg x + 110.1$ ,  $R^2 = 0.991$ ), whereas the conventional immunoassay (TMB substrate, procedure is described in the Supporting Information) had a 3.6-fold higher IC<sub>50</sub> of 6.5 ng/mL, a 12-fold higher LOD (IC<sub>10</sub>) of 0.73 ng/mL, and a smaller linear range from 1.7 to 25.2 ng/mL.

For a more practical use of the assay (naked-eye analysis), we designed an acrylamide concentration-dependent color indicator card (**Figure 4D**) for being used as on-site screening tool for rapid result analysis by the naked eye. For higher quantitative accuracy, which can be compromised by subjective deviations in human visual discrimination, we

also analyzed the RGB color codes of the digital images taken from the different solutions (**Supporting Figure S3**). Although all three colors (red, green, and blue or R, G, and B) showed acrylamide concentration-dependent intensity values, using B alone was most suitable for acrylamide quantification. Thus, we implemented the B value in the indicator card (**Figure 4D**) for more objective and user-friendlier (and also for weak-sighted and color-blind users) smartphone-assisted (using any RGB color value measurement application) acrylamide quantification. The proposed assay could be used to semi-quantitatively analyze acrylamide concentrations with the naked eye and/or a smartphone camera by using the color indicator card.

The specificity of the acrylamide immunoassay was evaluated by analyzing the cross-reactivity (CR) with five structurally related compounds, namely methyl carbamate, ethyl carbamate, acrylic acid, methyl acrylate, and methacrylamide, at a concentration of 1  $\mu\text{g/mL}$  after the same derivation reaction and with the derivatization reagent 9-xanthidrol at a concentration of 10  $\text{mg/mL}$ . The percentage of CR was calculated using the following equation:  $\text{CR (\%)} = [(\lambda_{\text{related\_analogues}} - \lambda_0) / (\lambda_{\text{acrylamide}} - \lambda_0)] \times 100$ , where  $\lambda_0$ ,  $\lambda_{\text{acrylamide}}$ , and  $\lambda_{\text{related\_analogues}}$  are the wavelengths of the longitudinal LSPR peaks of blank control, acrylamide, and related analogues, respectively.

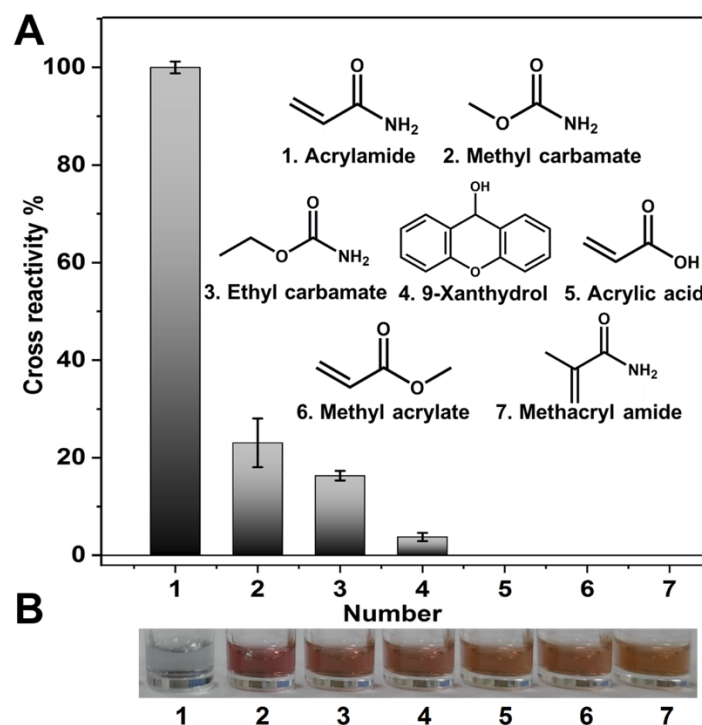


**Figure 5.** Specificity evaluation of multicolor immunoassay (A) and corresponding images (B) of solutions. Concentrations of the structurally related compounds was 1  $\mu\text{g/mL}$ . Concentration of 9-xanthidrol was 10  $\text{mg/mL}$ . Error bars show standard deviations ( $n = 3$ )

As shown in **Figure 5A**, acrylic acid, methyl acrylate, and methacryl amide showed negligible CR. Acrylic acid and methyl acrylate are lacking the necessary amide group for derivatization with 9-xanthidrol and are therefore not recognized by the mAb. Methacryl amide has the amide group but most probably the additional methyl group resulted in critical steric hindrance that prevented binding to the mAb. 9-xanthidrol showed 4% CR but due to its high concentration of 10  $\text{mg/mL}$ , this value can be considered as negligible influence on the analytical performance of the assay. Methyl carbamate and ethyl carbamate have very similar structures compared to acrylamide and the same derivatization

strategy can be used for ethyl carbamate immunoassays.<sup>40,41</sup> Therefore, it is not surprising that these two compounds show significant CRs of 23% (methyl carbamate) and 16% (ethyl carbamate). Despite the structural similarity, the CRs were still significantly lower compared to acrylamide, which showed the excellent specificity of the mAb for XAA binding. Moreover, methyl carbamate and ethyl carbamate are rarely found in acrylamide-containing samples,<sup>42</sup> which means that their CR will not influence the specific determination of acrylamide in the assay. The photos of the different solutions (**Figure 5B**) clearly showed that the sample colors of all CR compounds were orange and in strong contrast to the gray acrylamide sample color, which provided further evidence of the low affinity of the biot-mAb to these structurally related compounds and a concomitant strong Ag shell formation on the AuNRs.

To evaluate the reproducibility of the immunoassay, three samples with different concentrations of acrylamide were measured in triplicates by analyzing  $\Delta\lambda$  and the change of color. The standard deviations were below 7% for all samples, which confirmed the very good reproducibility of our multicolor acrylamide immunoassay (**Supporting Table S2**).

To highlight some pros and cons of our assay, we compared it to some recently developed acrylamide immunoassays (**Table 2**). Our multicolor immunoassay exhibited lower LODs than most of the other assays except one study that used polyclonal antibodies for the detection of acrylamide.<sup>16</sup> However, polyclonal antibodies exhibit significant drawbacks in production, leading to reduced specificity, considerable batch-to-batch differences, and

lower assay reproducibility. After careful screening, the mAb prepared in our study can overcome these drawbacks and provide high sensitivity combined with reproducible and reliable quantification of acrylamide. Most assays also require rather sophisticated instruments for acrylamide quantification. The carbon dot-based fluorescence immunoassay showed a calibration curve depending on a narrow mono-fluorescent signal variation range (0.21~6.48 ng/mL)<sup>20</sup> and signal measurement relied on a spectrophotometer. Electrochemical immunosensor<sup>43,44</sup> require the measurement of electrical signals and also chemiluminescence ELISAs<sup>18</sup> necessitate specific spectrometers for acrylamide detection. Conventional ELISAs<sup>15-17,19</sup> using TMB<sup>2+</sup> show simple color change from yellow to colorless, which is more prone to subjective deviations in human visual discrimination compared to our multicolor results for naked-eye or smartphone detection. However, no method is perfect and our multicolor immunoassay also has some shortcomings. Vivid colors produced by the deposition of Ag on AuNRs was implemented by relatively complicated experimental procedures including addition of AuNRs, AsAcP, and AgNO<sub>3</sub>. In addition, a precise quantitative analysis of multicolor assay requires screening of LSPR peaks, which can be time-consuming and also requires specific instruments.

**Table 2.** Comparison of available immunoassay methods for acrylamide analysis

Antibody	Method	Signal output	Sample	Pretreatment process	Linear range	LOD ng/mL <sup>a</sup> or ng/g <sup>b</sup>	Reference
Polyclonal antibody	Fluorescence immunoassay	Fluorescence	Water, cookies,	Hexane extraction	0.21-6.48 <sup>a</sup>	0.16 <sup>a</sup>	20







	Electrochemical immunosensor	Electrochemical signal	potato chips Coffee, cocoa, prune juice water,	Dilution or dissolution with PBS	10- 3.5*10 <sup>4a</sup>	3.84 <sup>a</sup>	44
	Electrochemical immunosensor	Electrochemical signal	coffee, potato chip	Solid phase extraction	4.74- 8.33 <sup>a</sup>	10 <sup>-3a</sup>	43
	ELISA	Absorbance	Potato chips, cookies, coffee	Hexane extraction	0.25- 24.15 <sup>b</sup>	0.036 <sup>b</sup>	16
	Chemiluminescence ELISA	Chemiluminescence	Instant noodles, cakes	PBS extraction	26.3- 221.1 <sup>a</sup>	18.6 <sup>a</sup>	18
	ELISA	Absorbance	Water	Solid phase extraction	51.76- 3311.5	65.7 <sup>b</sup>	19
	ELISA	Absorbance	Potato fries and biscuits	1.0% formic acid extraction	10-10 <sup>5a</sup>	6 <sup>a</sup>	17
	ELISA	Absorbance	Biscuits and cakes	Dilution with Deionized water	8.87- 112.92 <sup>a</sup>	8.87 <sup>a</sup>	15
Monoclonal antibody	Multicolor ELISA	Color change, UV-vis spectrum	Cookie, potato chips instant noodles, French fries	Hexane extraction	3 -172 <sup>b</sup>	0.6 <sup>b</sup>	This work

**Analysis of commercial food samples.** To test the applicability of our immunoassay to quantify acrylamide in actual food products, we selected a food product (instant noodles) with a known acrylamide concentration of 40.8 ng/g and spiked it with acrylamide

concentrations of 15, 30, 60, and 120 ng/g. It should be noted that due to pre-processing after sample extraction using a 10-fold dilution, the LOD of the actual sample analysis was increased to 0.6 ng/g and the linear range became 3 to 172 ng/g. However, the analytical performance should still be sufficient and in addition, the dilution can significantly reduce sample matrix effects, which was confirmed by the results of the recovery test. Using the same derivatization conditions as for the standard curve, the obtained recovery was in the range of 84% to 102% with coefficients of variation between 7% and 9% (**Table 3**). Importantly, based on the color change of the spiked samples and using the color indicator card, the acrylamide concentration ranges could be obtained by naked-eye and smartphone analyses, which were consistent with the UV-vis analysis results.

**Table 3.** Recovery analysis of food samples (instant noodles) by multicolor immunoassay ( $n=3$ ).

Original acrylamide conc.(ng/g)	Spiking level (ng/g)	Naked-eye / smartphone		UV-vis	Recovery (%)	CV <sup>b</sup> (%)
		Photograph	Indicator analysis (ng/g)	Mean $\pm$ SD <sup>a</sup> (ng/g)		
40.8	15	 B <sub>mean</sub> =156 <sup>c</sup>	20-54	53.3 $\pm$ 4.2	83.4	7.9
	30	 B <sub>mean</sub> =162	54-125	68 $\pm$ 5.6	90.6	8.3
	60	 B <sub>mean</sub> =169	54-125	99.4 $\pm$ 8.7	97.6	8.7
	120	 B <sub>mean</sub> =173	>125	162.8 $\pm$ 11.3	101.7	6.9

<sup>a</sup> Standard deviation; <sup>b</sup> Coefficient of variation; <sup>c</sup> Average blue (B) value of RGB image obtained from a smartphone ( $n=3$ ).

For going a step further in evaluating the applicability of the assay for food sample analysis, ten different food products were collected randomly from a local market and analyzed by UV-vis spectroscopy, color indication (using the color indicator card), and UPLC-Q-Orbitrap HRMS as standard method. As shown in **Table 4**, there was an excellent agreement between the different methods, which confirmed the applicability of our multicolor immunoassay for accurate acrylamide analysis in different typical food products. Notably, even after the 10-fold dilution in our assays, samples 1, 3, 6, 8, and 9 contained acrylamide concentrations that exceeded the upper limit of quantification with UV-vis (172 ng/g). Still these samples could be identified as high acrylamide concentration samples by both UV-vis and color indicator analysis. However, additional dilution would be necessary for a more exact quantification of these highly concentrated samples. Another interesting finding was the relatively low concentration of acrylamide in samples 5 and 7. In fact, the packaging information indicated that the production of these two samples avoided high-temperature frying, such that the generation of acrylamide should also be avoided, as confirmed by our measurements. Although UPLC-Q-Orbitrap HRMS resulted in a significantly more accurate quantification compared to our semiquantitative analysis, it required expensive instrumentation and highly trained personnel. Independent sample analysis mode (8 min/sample) also leads to low efficiency for the screening of a large number of samples via UPLC-Q-Orbitrap HRMS. The proposed multicolor immunoassay with high throughput capability, simplicity, and straightforward readout is a highly

complementary method to UPLC-Q-Orbitrap HRMS because it provides the possibility of simple and userfriendly monitoring of acrylamide concentrations in most fried food products with excellent analytical performance and applicability.

**Table 4.** Comparison of the blind analysis results for acrylamide content in food samples by immunoassay ( $n=3$ ) and UPLC-Q-Orbitrap HRMS.

Sample	Immunoassay		UPLC-Q-Orbitrap HRMS (ng/g)
	UV-Vis analysis, Mean $\pm$ SD (ng/g)	Indicator analysis (ng/g) <sup>b</sup>	
NO.1 (Cookies)	>172 <sup>a</sup>	>125	959.8
NO.2 (Cookies)	126.7 $\pm$ 1.2	>125	128.0
NO.3 (Potato chips)	>172	>125	369.6
NO.4 (Cookies)	72.5 $\pm$ 3.7	54-125	74.8
NO.5 (Potato chips)	45.8 $\pm$ 1.4	20-54	45.4
NO.6 (Cookies)	>172	>125	499.3
NO.7 (Instant noodles)	41.2 $\pm$ 1.1	20-54	40.8
NO.8 (French fries)	>172	>125	406.2
NO.9 (Cookies)	>172	>125	647.7
NO.10 (Cookies)	83.0 $\pm$ 1.1	54-125	84.5

<sup>a</sup> Upper limit of quantitation (172 ng/g); <sup>b</sup> Corresponding images are shown in Supporting Table S3.

## CONCLUSIONS

In summary, we successfully designed, characterized, and applied a multicolor immunoassay for the determination of acrylamide in fried food samples. The assay

principle was based on specifically developed monoclonal antibodies that recognized xanthyl acrylamide and competitive binding that was used for tuning the thickness of Ag shells on AuNRs via ALP-induced silver deposition. The strong acrylamide concentration-dependent color change resulted in excellent assay performance and a very low detection limit of 0.06 ng/g, which allowed us to use a 10-fold dilution of food samples to suppress sample matrix effects. In addition to quantification via UV-vis spectroscopy, the assay demonstrated rapid, sensitive, and specific quantification of acrylamide in various different food samples by naked-eye or smartphone color detection as verified by UPLC-Q-Orbitrap HRMS. The present assay also possessed very good stability and reproducibility, which provides a powerful and simple screening strategy for risk monitoring and exposure assessment of acrylamide in common food samples.

## **ACKNOWLEDGEMENTS**

This work was supported by the National Nature Science Foundation of China (31822039, 31972157), the Special Support Program of Guangdong Province, China (2019TX05N052), the Brain Pool program funded by the Ministry of Science and ICT through the National Research Foundation of Korea (2021H1D3A2A0204958912), Seoul National University, Université Paris-Saclay, Université de Rouen Normandie, INSA Rouen Normandie, CNRS, European Regional Development Fund, Labex SynOrg (ANR-11-LABX-0029), Carnot Institute I2C, XL-Chem graduate school (ANR-18-EURE-0020

XL CHEM), and the Region Normandie. Hui-Jun Fu was supported by a China Scholarship Council (CSC) scholarship to visit Université de Rouen Normandie.

## NOTES

The authors declare no conflict of interest.

## REFERENCES

- (1) Stadler, R. H.; Blank, I.; Varga, N.; Robert, F.; Hau, J.; Guy, P. A.; Robert, M. C.; Riediker, S., Acrylamide from Maillard reaction products. *Nature* **2002**, 419, (6906), 449-50.
- (2) Salimi, A.; Baghal, E.; Ghobadi, H.; Hashemidanesh, N.; Khodaparast, F.; Seydi, E., Mitochondrial, lysosomal and DNA damages induced by acrylamide attenuate by ellagic acid in human lymphocyte. *PLoS One* **2021**, 16, (2), e0247776.
- (3) Paulsson, B.; Kotova, N.; Grawe, J.; Henderson, A.; Granath, F.; Golding, B.; Tornqvist, M., Induction of micronuclei in mouse and rat by glycidamide, genotoxic metabolite of acrylamide. *Toxicol Environ. Mutagen.* **2003**, 535, (1), 15-24.
- (4) Klaunig, J. E., Acrylamide Carcinogenicity. *J. Agr. Food Chem.* **2008**, 56, (15), 5984-5988.
- (5) Besaratinia, A.; Pfeifer, G. P., A review of mechanisms of acrylamide carcinogenicity. *Carcinogenesis* **2006**, 28, (3), 519-528.
- (6) Yang, L.; Dong, L.; Zhang, L.; Bai, J.; Chen, F.; Luo, Y., Acrylamide Induces Abnormal mtDNA Expression by Causing Mitochondrial ROS Accumulation, Biogenesis, and Dynamics Disorders. *J. Agr. Food Chem.* **2021**, 69, (27), 7765-7776.
- (7) LoPachin, R. M., The changing view of acrylamide neurotoxicity. *Neurotoxicology* **2004**, 25, (4), 617-30.
- (8) International Agency for Research on Cancer. IARC Monographs on the Evaluation of Carcinogenic Risks to Humans. Volume 60: Some Industrial Chemicals. 1994
- (9) Tareke, E.; Rydberg, P.; Karlsson, P.; Eriksson, S.; Törnqvist, M., Analysis of Acrylamide, a Carcinogen Formed in Heated Foodstuffs. *J. Agr. Food Chem.* 2002, 50, (17), 4998-5006.
- (10) FDA, Guidance for Industry Acrylamide in Foods. 2016,.
- (11) Commission, E., Commission Regulation (EU) 2017/ 2158 of 20 November 2017 establishing mitigation

measures and benchmark levels for the reduction of the presence of acrylamide in food. In 2017; Vol. 304, pp 24–44.

(12) Milkovska-Stamenova, S.; Schmidt, R.; Frolov, A.; Birkemeyer, C., GC-MS Method for the Quantitation of Carbohydrate Intermediates in Glycation Systems. *J. Agr. Food Chem.* **2015**, *63*, (25), 5911-5919.

(13) Elahi, M.; Kamankesh, M.; Mohammadi, A.; Jazaeri, S., Acrylamide in Cookie Samples: Analysis Using an Efficient Co-Derivatization Coupled with Sensitive Microextraction Method Followed by Gas Chromatography-Mass Spectrometry. *Food Anal. Method.* **2019**, *12*, (6), 1439-1447.

(14) Assaat, L.; Saepudin, E.; Soejoedono, R.; Adji, R.; Poetri, O.; Ivandini, T., Production of a polyclonal antibody against acrylamide for immunochromatographic detection of acrylamide using strip tests. *J. Appl. Anim. Res.* **2019**, *6*, (3), 366.

(15) Zhu, Y.; Song, S.; Liu, L.; Kuang, H.; Xu, C., An indirect competitive enzyme-linked immunosorbent assay for acrylamide detection based on a monoclonal antibody. *Food Agr. Immunol.* **2016**, *27*, (6), 796-805.

(16) Wu, J.; Shen, Y.; Lei, H.; Sun, Y.; Yang, J.; Xiao, Z.; Wang, H.; Xu, Z., Hapten Synthesis and Development of a Competitive Indirect Enzyme-Linked Immunosorbent Assay for Acrylamide in Food Samples. *J. Agr. Food Chem.* **2014**, *62*, (29), 7078-7084.

(17) Zhou, S.; Zhang, C.; Wang, D.; Zhao, M., Antigen synthetic strategy and immunoassay development for detection of acrylamide in foods. *The Analyst* **2008**, *133*, (7), 903.

(18) Quan, Y.; Chen, M.; Zhan, Y.; Zhang, G., Development of an Enhanced Chemiluminescence ELISA for the Rapid Detection of Acrylamide in Food Products. *J. Agr. Food Chem.* **2011**, *59*, (13), 6895-6899.

(19) Preston, A.; Fodey, T.; Elliott, C., Development of a high-throughput enzyme-linked immunosorbent assay for the routine detection of the carcinogen acrylamide in food, via rapid derivatisation pre-analysis. *Anal. Chim. Acta* **2008**, *608*, (2), 178-185.

(20) Luo, L.; Jia, B.; Wei, X.; Xiao, Z.; Wang, H.; Sun, Y.; Shen, Y.; Lei, H.; Xu, Z., Development of an inner filter effect-based fluorescence immunoassay for the detection of acrylamide using 9-xanthidrol derivatization. *Sens. Actuators B Chem.* **2021**, *332*, 129561.

(21) Fu, H.; Wang, Y.; Xiao, Z.; Wang, H.; Li, Z.; Shen, Y.; Lei, H.; Sun, Y.; Xu, Z.; Hammock, B., A rapid and simple fluorescence enzyme-linked immunosorbent assay for tetrabromobisphenol A in soil samples based on a bifunctional fusion protein. *Ecotox. Environ. Safe.* **2020**, *188*, 109904.

(22) Fu, H.; Yuan, L.; Shen, Y.; Liu, Y.; Liu, B.; Zhang, S.; Xie, Z.; Lei, H.; Sun, Y.; Xu, Z., A full-automated magnetic particle-based chemiluminescence immunoassay for rapid detection of cortisol in milk. *Anal. Chim. Acta* **2018**, *1035*, 129-135.

(23) Xiong, L.; He, X.; Xia, J.; Ma, H.; Yang, F.; Zhang, Q.; Huang, D.; Chen, L.; Wu, C.; Zhang, X.; Zhao, Z.; Wan, C.; Zhang, R.; Cheng, J., Highly Sensitive Naked-Eye Assay for Enterovirus 71 Detection Based

on Catalytic Nanoparticle Aggregation and Immunomagnetic Amplification. *ACS Appl. Mater. Inter.* **2017**, 9, (17), 14691-14699.

(24) Huang, Y.; Lin, Y.; Luo, F.; Wang, P.; Wang, J.; Qiu, B.; Guo, L.; Lin, Z., Rapid detection of dibutyl phthalate in liquor by a semi-quantitative multicolor immunosensor with naked eyes as readout. *Anal. Methods-UK* **2019**, 11, (4), 524-529.

(25) Peng, L.; Li, B. L.; Zhou, C. W.; Li, N. B.; Setyawati, M. I.; Zou, H. L., “Naked-eye” recognition: Emerging gold nano-family for visual sensing. *Appl. Mater. Today* **2018**, 11, 166-188.

(26) Liu, Y.; Zhang, Z.; Yu, J.; Xie, J.; Li, C. M., A concentration-dependent multicolor conversion strategy for ultrasensitive colorimetric immunoassay with the naked eye. *Anal. Chim. Acta* **2017**, 963, 129-135.

(27) Ma, X.; Lin, Y.; Guo, L.; Qiu, B.; Chen, G.; Yang, H.; Lin, Z., A universal multicolor immunosensor for semiquantitative visual detection of biomarkers with the naked eyes. *Biosensors and Bioelectronics* **2017**, 87, 122-128.

(28) Liu, D.; Zhang, Y.; Zhu, M.; Yu, Z.; Ma, X.; Song, Y.; Zhou, S.; Yang, C., Microfluidic-Integrated Multicolor Immunosensor for Visual Detection of HIV-1 p24 Antigen with the Naked Eye. *Anal. Chem.* **2020**, 92, 11826-11833.

(29) Ma, X.; Chen, Z.; Kannan, P.; Lin, Z.; Qiu, B.; Guo, L., Gold Nanorods as Colorful Chromogenic Substrates for Semiquantitative Detection of Nucleic Acids, Proteins, and Small Molecules with the Naked Eye. *Anal. Chem.* **2016**, 88, (6), 3227-34.

(30) Xu, S.; Ouyang, W.; Xie, P.; Lin, Y.; Qiu, B.; Lin, Z.; Chen, G.; Guo, L., Highly Uniform Gold Nanobipyramids for Ultrasensitive Colorimetric Detection of Influenza Virus. *Anal. Chem.* **2017**, 89, 1617-1623.

(31) Gao, X. Y. A. Z., Enzyme-catalysed deposition of ultrathin silver shells on gold nanorods: a universal and highly efficient signal amplification strategy for translating immunoassay into a litmus-type test. *Chem. Comm.* **2015**, 51, 6928-6931.

(32) Liu, Y.; Wang, J.; Zhao, C.; Guo, X.; Song, X.; Zhao, W.; Liu, S.; Xu, K.; Li, J., A multicolorimetric assay for rapid detection of *Listeria monocytogenes* based on the etching of gold nanorods. *Anal. Chim. Acta* **2019**, 1048, 154-160.

(33) Fang, B.; Xu, S.; Huang, Y.; Su, F.; Huang, Z.; Fang, H.; Peng, J.; Xiong, Y.; Lai, W., Gold nanorods etching-based plasmonic immunoassay for qualitative and quantitative detection of aflatoxin M1 in milk. *Food Chem.* **2020**, 329, 127160.

(34) Li, M.; Ding, C.; Jia, P.; Guo, L.; Wang, S.; Guo, Z.; Su, F.; Huang, Y., Semi-quantitative detection of p-Aminophenol in real samples with colorfully naked-eye assay. *Sens. Actuators B Chem.* **2021**, 334, 129604.

(35) Li, D.; Cui, Y.; Morisseau, C.; Gee, S. J.; Bever, C. S.; Liu, X.; Wu, J.; Hammock, B. D.; Ying, Y., Nanobody Based Immunoassay for Human Soluble Epoxide Hydrolase Detection Using Polymeric



Horseradish Peroxidase (PolyHRP) for Signal Enhancement: The Rediscovery of PolyHRP? *Anal. Chem.* **2017**, 89, (11), 6248-6256.

(36) Rodríguez-Lorenzo, L.; Romo-Herrera, J. M.; Pérez-Juste, J.; Alvarez-Puebla, R. A.; Liz-Marzán, L. M., Reshaping and LSPR tuning of Au nanostars in the presence of CTAB. *J. Mater. Chem.* **2011**, 21, 11544.

(37) Wei, J.; Chang, W.; Qileng, A.; Liu, W.; Zhang, Y.; Rong, S.; Lei, H.; Liu, Y., Dual-Modal Split-Type Immunosensor for Sensitive Detection of Microcystin-LR: Enzyme-Induced Photoelectrochemistry and Colorimetry. *Anal. Chem.* **2018**, 90, (15), 9606-9613.

(38) Wang, F.; Na, N.; Ouyang, J., A catalytic—regulated gold nanorods etching process as a receptor with multiple readouts for protein detection. *Sens. Actuators B Chem.* **2020**, 318, 128215.

(39) Tian, F.; Zhou, J.; Fu, R.; Cui, Y.; Zhao, Q.; Jiao, B.; He, Y., Multicolor colorimetric detection of ochratoxin A via structure-switching aptamer and enzyme-induced metallization of gold nanorods. *Food Chem.* **2020**, 320, 126607.

(40) Luo, L.; Lei, H.; Yang, J.; Liu, G.; Sun, Y.; Bai, W.; Wang, H.; Shen, Y.; Chen, S.; Xu, Z., Development of an indirect ELISA for the determination of ethyl carbamate in Chinese rice wine. *Anal. Chim. Acta* **2017**, 950, 162-169.

(41) Fu, H.; Chen, Z.; Wang, H.; Luo, L.; Wang, Y.; Huang, R.; Xu, Z.; Hammock, B., Development of a sensitive non-competitive immunoassay via immunocomplex binding peptide for the determination of ethyl carbamate in wine samples. *J. Hazard. Mater.* **2021**, 406, 124288.

(42) Sen, N. P.; Seaman, S. W.; Boyle, M.; Weber, D., Methyl carbamate and ethyl carbamate in alcoholic beverages and other fermented foods. *Food Chemistry* **1993**, 48, 359-366.

(43) Wu, M.; Wang, Y.; Li, S.; Dong, X.; Yang, J.; Shen, Y.; Wang, H.; Sun, Y.; Lei, H.; Xu, Z., Ultrasensitive immunosensor for acrylamide based on chitosan/SnO<sub>2</sub>-SiC hollow sphere nanochains/gold nanomaterial as signal amplification. *Anal. Chim. Acta* **2019**, 1049, 188-195.

(44) Lau, P. Y.; Ng, K. L.; Yusof, N. A.; Liu, G.; Alias, Y.; Khor, S. M., A sample pre-treatment free electrochemical immunosensor with negative electro-pulsion for quantitative detection of acrylamide in coffee, cocoa and prune juice. *Anal. Methods-UK* **2019**, 11, (33), 4299-4313.

# Table of Contents graphic

